

STRUCTURE FUNCTIONS OF NUCLEI AT SMALL x AND DIFFRACTION AT HERA

by

A. Capella, A. Kaidalov*, C. Merino**, D. Pertermann *** and J. Tran Thanh Van

Laboratoire de Physique Théorique et Hautes Energies ****
Université de Paris XI, bâtiment 211, 91405 Orsay cedex, France

Abstract

Gribov theory is applied to investigate the shadowing effects in the structure functions of nuclei. In this approach these effects are related to the process of diffractive dissociation of a virtual photon. A model for this diffractive process, which describes well the HERA data, is used to calculate the shadowing in nuclear structure functions. A reasonable description of the x , Q^2 and A -dependence of nuclear shadowing is achieved.

LPTHE Orsay 97-04

February 1997

* Permanent address : ITEP, B. Cheremushkinskaya 25, 117259 Moscow, Russia

** Permanent address : Universidade Santiago de Compostela, Dep. Física de Partículas, E-15706 Santiago de Compostela, Spain

*** Permanent address : Univ-GH-Siegen, Phys. Dept., D-57068 Siegen, Germany

**** Laboratoire associé au Centre National de la Recherche Scientifique - URA D0063

1. Introduction

Deep inelastic scattering (DIS) on nuclei gives important information on distributions of quarks and gluons in nuclei. The region of small Bjorken x is especially interesting because partonic clouds of different nucleons overlap as $x \rightarrow 0$ and shadowing effects become important. There are experimental results in this region, which show that there are strong deviations from an A^1 behavior in the structure functions [1]. Several theoretical models have been proposed to understand these data [1]. The most general approach is based on the Gribov method [2]. It relates partonic and hadronic descriptions of small x phenomena in interactions of real or virtual photons with nuclei. In this approach the shadowing effects can be expressed in terms of the cross-sections for diffraction dissociation of a photon on a nucleon (Fig. 1). This process has been studied recently in DIS at HERA [3]. The detailed x , Q^2 and M^2 (M is the invariant mass of the diffractively produced system) dependencies observed in these experiments [3] have been well described in the theoretical model of ref. [4] which is based on Regge factorizations and uses as an input available information on diffractive production in hadronic interactions. Here we will apply the same model to calculate the structure functions of nuclei in the small x -region. The use of the model, which describes well the diffraction dissociation of virtual photons on a nucleon target, leads to a strong reduction of the theoretical uncertainty in calculations of the structure functions of nuclei in comparison with previous calculations [1, 5].

2. The model

In the Gribov approach the forward scattering amplitude of a photon with virtuality Q^2 on a nuclear target can be written as the sum of the diagrams shown in Fig. 2. The diagram of Fig. 2a corresponds to the sum of interactions with individual nucleons and is proportional to A^1 . The second diagram (2b) contains a double scattering with two target

nucleons. It gives a negative contribution to the total cross-section, proportional to $A^{4/3}$ (for large A) and describes the shadowing effects for sea quarks. According to reggeon diagram technique [6] and Abramovsky, Gribov, Kancheli (AGK) cutting rules [7], the contribution of the diagram of Fig. 2b to the total γ^* - A cross-section is related to the diffractive production of hadrons by a virtual photon as follows :

$$\sigma_A^{(2)} = -4\pi A(A-1) \int d^2b T_A^2(b) \int dM^2 \left. \frac{d\sigma_{\gamma^*p}^{\mathcal{D}}}{dM^2 dt} \right|_{t=0} F_A(t_{min}) \quad , \quad (1)$$

where $T_A(b)$ is the nuclear profile function, ρ_A is the nucleon density ($T_A(b) = \int_{-\infty}^{+\infty} dZ \rho_A(b, Z)$, $\int d^2b T_A(b) = 1$) and

$$F_A(t_{min}) = \int dZ e^{-iq_Z Z} \rho_A(b, Z) / T_A(b) \quad , \quad t_{min} = -q_Z^2 = -m_N^2 x^2 \left(\frac{Q^2}{M^2 + Q^2} \right)^{-2} \quad .$$

Note that $F_A(t_{min})$ is equal to unity as $x \rightarrow 0$ and decreases fast as x increases to $x_{cr} \sim \frac{1}{m_N R_A}$, due to a lack of coherence for $x > x_{cr}$.

Thus the second order rescattering term can be calculated if the differential cross-section for diffractive production by a virtual photon is known.

Higher order rescatterings are model dependent, but in the region of $x \gtrsim 10^{-3}$, where experimental data exist, their contribution is rather small (\sim several %) for existing nuclei. We use the following unitary expression for the total γ^* - A cross-section

$$\sigma_{\gamma^*A} = \sigma_{\gamma^*N} \int d^2b \frac{A T_A(b)}{1 + (A-1)f(x, Q^2)T_A(b)} \quad (2)$$

where

$$f(x, Q^2) = 4\pi \int dM^2 \left. \frac{d\sigma_{\gamma^*p}^{\mathcal{D}}}{dM^2 dt} \right|_{t=0} F_A(t_{min}) / \sigma_{\gamma^*N} \quad .$$

This expression is valid in the generalized Schwimmer model [8, 9] and corresponds to the summation of fan diagrams with triple Pomeron interaction. We have checked that the results for eikonal-type summation of higher order rescatterings are very similar to the one obtained with (2).

Thus we obtain for the ratio $R_A = F_{2A}/F_{2N}$, in the region of small x

$$\frac{F_{2A}}{F_{2N}} = \int d^2b \frac{A T_A(b)}{1 + (A-1)f(x, Q^2)T_A(b)} \quad . \quad (3)$$

The deviation of this ratio from $A^1 = A \int d^2b T_A(b)$ is due to the second term in the denominator of the integrand in eq. (3). Thus, knowing the differential cross-section for diffraction dissociation on a nucleon and the structure function of a nucleon (σ_{γ^*N}), one can predict the A (and x, Q^2) dependence of structure functions of nuclei. Eq. (3) can only be used in the region $x < 10^{-1}$ where the sea quarks component dominates, because at larger values of x shadowing of valence quarks (which in general is not described by eq. (3)) becomes important [10, 11]. The effects which lead to antishadowing are also important in the region of $x \sim 0.1$.

In refs [4] we described the diffractive contribution to DIS in terms of Pomeron exchange

$$F_2^{\mathcal{D}}(x, Q^2, x_P, t) = \frac{(g_{pp}^P(t))^2}{16\pi} x_P^{1-2\alpha_P(t)} F_P(\beta, Q^2, t) \quad (4)$$

where $g_{pp}^P(t)$ is the Pomeron-proton coupling ($g_{pp}^P(t) = g_{pp}^P(0) \exp(Ct)$ with $(g_{pp}^P(0))^2 = 23 \text{ mb}$ and $C = 2.2 \text{ GeV}^{-2}$), $\alpha_P(t)$ is the Pomeron trajectory ($\alpha_P(0) = 1.13$, $\alpha'_P(0) = 0.25 \text{ GeV}^{-2}$) and $F_P(\beta, Q^2, t)$ is the Pomeron structure function. The variable $\beta = \frac{Q^2}{M^2 + Q^2} = \frac{x}{x_P}$ plays the same role for the Pomeron as the Bjorken variable x for the proton. At large Q^2 , F_P can be expressed in terms of the quark distribution in the Pomeron

$$F_P(\beta, Q^2, t) = \sum_i e_i^2 \beta [q_i^P(\beta, Q^2, t) + \bar{q}_i^P(\beta, Q^2, t)] \quad . \quad (5)$$

In refs. [4] we determined $F_P(\beta, Q^2, t)$ using Regge-factorization for small values of β and a plausible assumption on the $\beta \rightarrow 1$ behavior. This function was then used as an initial condition for QCD evolution of partons in the Pomeron. The results of the QCD-evolution crucially depend on the form of the gluon distribution in the Pomeron. Experimental results for $F_2^{\mathcal{D}}$ can be understood only if the distribution of gluons in the Pomeron is rather hard and the gluons carry the main part of the Pomeron momentum [4, 12-14].

The model described above gives a reasonable description of the process of diffractive production in DIS and can be used to compute the function $f(x, Q^2)$, which determine the shadowing of nuclear structure function via (3). This function can be written in terms of the ratio F_P/F_{2N} :

$$f(x, Q^2) = \int \frac{d\beta}{4\beta} (g_{pp}^P(0))^2 \left(\frac{1}{x_P} \right)^{2\Delta} \frac{F_P(\beta, Q^2)}{F_{2N}(\beta, Q^2)} F_A(t_{min}) \quad (6)$$

where the integral limits are x/x_{0P} with $x_{0P} = 0.1$ and $Q^2/(m_\rho^2 + Q^2)$. For the nucleon structure function F_{2N} we use the results of ref. [15] and for $F_P(\beta, Q^2)$ the expression and parameters of ref. [4b]. In the numerical calculations we use a standard Woods-Saxon profile for $A > 20$ and a gaussian for $A < 20$ with a rms radius given by $R_A = 0.82A^{1/3} + 0.58$ fm [16]. For deuteron we have also used a gaussian with an artificially high radius in order to reproduce the small amount of shadowing present in this case. The results of our calculations are shown in Figs. 3-7.

3. Numerical results

Comparison of our predictions for the ratio $\frac{2}{A}F_{2A}/F_2^D$ with experimental data of NMC [17] is shown in Fig. 3 and for ratios of different nuclei in Fig. 4. New data for the ratio $F_2^{S_n}/F_2^C$ [18] are also shown in Fig. 4. It is important to note that experimental points in Figs. 3, 4 for different x correspond to different values of $\langle Q^2 \rangle$ [17] [18]. This correlation has been taken into account in our calculations. The agreement between theoretical predictions and experimental data is rather good taking into account that there are no free parameter in our calculations. However, one should notice that for large nuclei (S_n), the onset of the shadowing seems to move to smaller values of x as compared to light ones. This trend is also present in the Pb data of ref. [19] and is not reproduced in our model (despite the decrease of x_{crit} with increasing A). This probably indicates that antishadowing (not present in our model) extends to smaller x values for heavier nuclei.

Our predictions for the ratio $\frac{1}{A} \frac{F_{2A}}{F_{2N}}$ in the region of very small x are shown in Figs. 5

for fixed values of Q^2 . They can be confronted to experiment if nuclei at HERA will be available. Note that our results are more reliable for small values of x ($x < 10^{-2}$) where the effects of both valence quark shadowing and antishadowing are negligible. The curves for shadowing effects in the gluon distribution of nuclei $\frac{1}{A} \frac{g^A(x, Q^2)}{g^N(x, Q^2)}$ are shown in Figs. 6. They look similar to the shadowing for the quark case. However the absolute magnitude of the shadowing is smaller in the gluon case contrary to expectations of some theoretical models [1] but in agreement with [20]. (Note that these results are sensitive to the gluonic distribution in the Pomeron, which is poorly known at present). These predictions can be tested in experimental studies of J/ψ and Υ -production on nuclear targets at RHIC and LHC.

Finally we want to discuss in more detail the Q^2 -dependence of the shadowing. Recent NMC data [18] for the ratio of $F_2^{S_n}/F_2^C$ are shown in Figs. 7 as functions of Q^2 for fixed values of x in the small x region. The theoretical curves have a weak dependence on Q^2 and are in a reasonable agreement with experiment, although the Q^2 dependence seems stronger in the data especially in the region of small Q^2 . At larger values of x the data are practically Q^2 -independent. These properties should be checked in future experiments.

4. Conclusions

In conclusion, a model based on the Gribov-Glauber theory of nuclear shadowing and the properties of diffraction in DIS observed at HERA, leads to a fair description of experimental data on structure functions of nuclei in the small x region. Predictions of shadowing effects for quark and gluon distributions are given. They can be tested in future experiments at HERA and in hadronic colliders.

Acknowledgements

One of us (A.C.) would like to thank G. Do Dang for discussions. A. K. and D. P. wish

to thank the LPTHE for hospitality during a period when this work was initiated. The work has been partially supported by grant 93-0079 of INTAS. A. K. also acknowledges support from the grant N° 96-02-19184 of RFFI.

References

- [1] M. Arneodo, Phys. Reports **240** (1994) 301 (and references therein).
- [2] V. N. Gribov, ZhETF **56** (1969) 892, *ibid* **57** (1969) 1306 [Sov. Phys. JETP **29** (1969) 483, **30** (1970) 709].
- [3] T. Ahmed et al (H1 collaboration), Phys. Lett. **B348** (1995) 681.

M. Derrick et al (Zeus collaboration), Z. Phys. **C68** (1995) 569 ; Z. Phys. **C70** (1996) 391.
- [4] a) A. Capella, A. Kaidalov, C. Merino and J. Tran Thanh Van, Phys. Lett. **B343** (1995) 403.

b) A. Capella, A. Kaidalov, C. Merino, D. Pertermann and J. Tran Thanh Van, Phys. Rev. **D53** (1996) 2309.
- [5] K. Boreskov, A. Capella, A. Kaidalov and J. Tran Thanh Van, Phys. Rev. **D47** (1993) 219.
- [6] V. N. Gribov, ZhETF **57** (1967) 654 [Sov. Phys. JETP **26** (1968) 14].
- [7] V. A. Abramovsky, V. N. Gribov and O. V. Kancheli, Yad. Fiz. **18** (1973) 595 [Sov. J. Nucl. Phys. **18** (1974) 308].
- [8] A. Schwimmer, Nucl. Phys. **B94** (1975) 445.
- [9] K. G. Boreskov et al., Yad. Fiz. **53** (1991) 569 [Sov. J. Nucl. Phys. **53** (1991) 356].
- [10] L. L. Frankfurt, M. I. Strikman and S. Liuti, Phys. Rev. Lett. **65** (1990) 1725.
- [11] A. B. Kaidalov, C. Rasinariu and U. Sukhatme, UICHEP-TH/96-9.
- [12] T. Gehrmann and W. J. Stirling, Z. Phys. **C70** (1996) 89.
- [13] K. Golec-Biernat and J. Kwiecinski, Phys. Lett. **B353** (1995) 329.

- [14] J. Dainton (H1 collaboration), Proceedings Workshop on Deep Inelastic Scattering and QCD, Paris, France, 24-28 April 1995 (ed. J. P. Laporte and Y Sirois).
- [15] A. Capella, A. Kaidalov, C. Merino, J. Tran Thanh Van, Phys. Lett **B337** (1994) 358.
- [16] M. A. Preston and R. K. Bhoduri, Structure of the Nucleus, Addison-Wesley, New York 1975.
- [17] P. Amandruz et al (NMC collaboration), Nucl. Phys. **B441** (1995) 3.
- [18] N. Arneodo et al (NMC collaboration), Nucl. Phys. **B481** (1996) 23.
- [19] M. R. Adams et al (E665 collaboration), Z. Phys. **C67** (1995) 407.
- [20] K. J. Eskola, Nucl. Phys. **B400** (1994) 240.

Figure Captions

Fig. 1 : Diffractive dissociation of a virtual photon. The shaded area represents the exchange of a Pomeron.

Fig. 2 : The first two terms (single and double scattering) of the multiple scattering series for the total γ^*N cross-section in the Gribov-Glauber approach.

Fig. 3 : The ratios $(2/A)F_2^A/F_2^D$ computed from eq. (3) for different values of x . The experimental points are from ref. [17]. The values of Q^2 are different for different x -values [17].

Fig. 4 : The ratios $(A_1/A_2)F_2^{A_2}/F_2^{A_1}$ computed from eq. (3) for different values of x . The experimental points are from refs. [17] and [18]. The values of Q^2 are different for different x values [17, 18].

Fig. 5 : The ratios $(1/A)F_2^A/F_2^N$ computed from eq. (3) for different values of x in the small x region, at fixed values of Q^2 .

Fig. 6 : The ratios $(1/A_2)g^A/g^N$ of gluon distribution functions computed for different values of x in the low x region, at fixed values of Q^2 .

Fig. 7 : The ratio $(12/119)F_2^{S_n}/F_2^C$ computed from eq. (3) for different values of Q^2 , at two fixed values of x . The data points are from ref. [18].

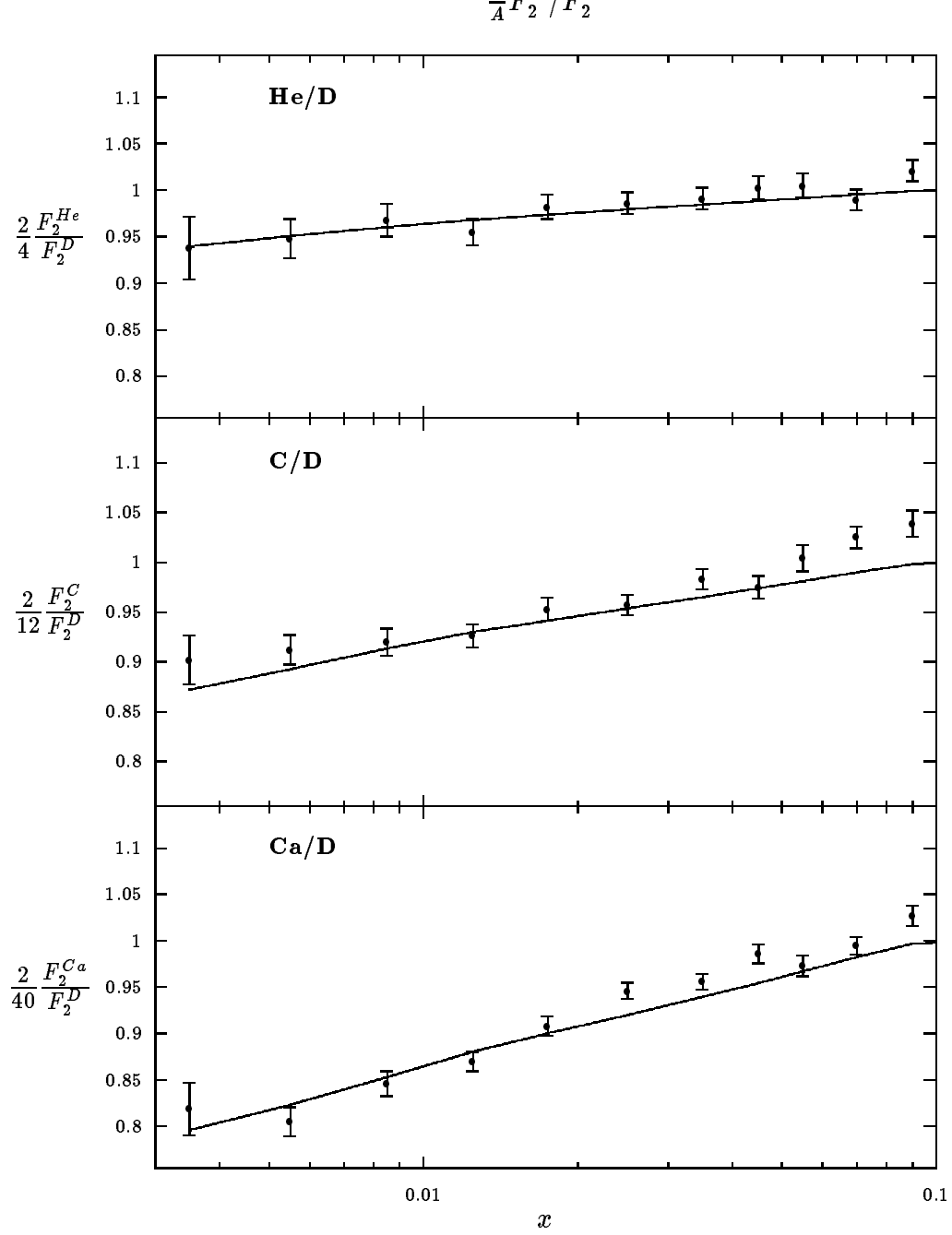


Fig. 3

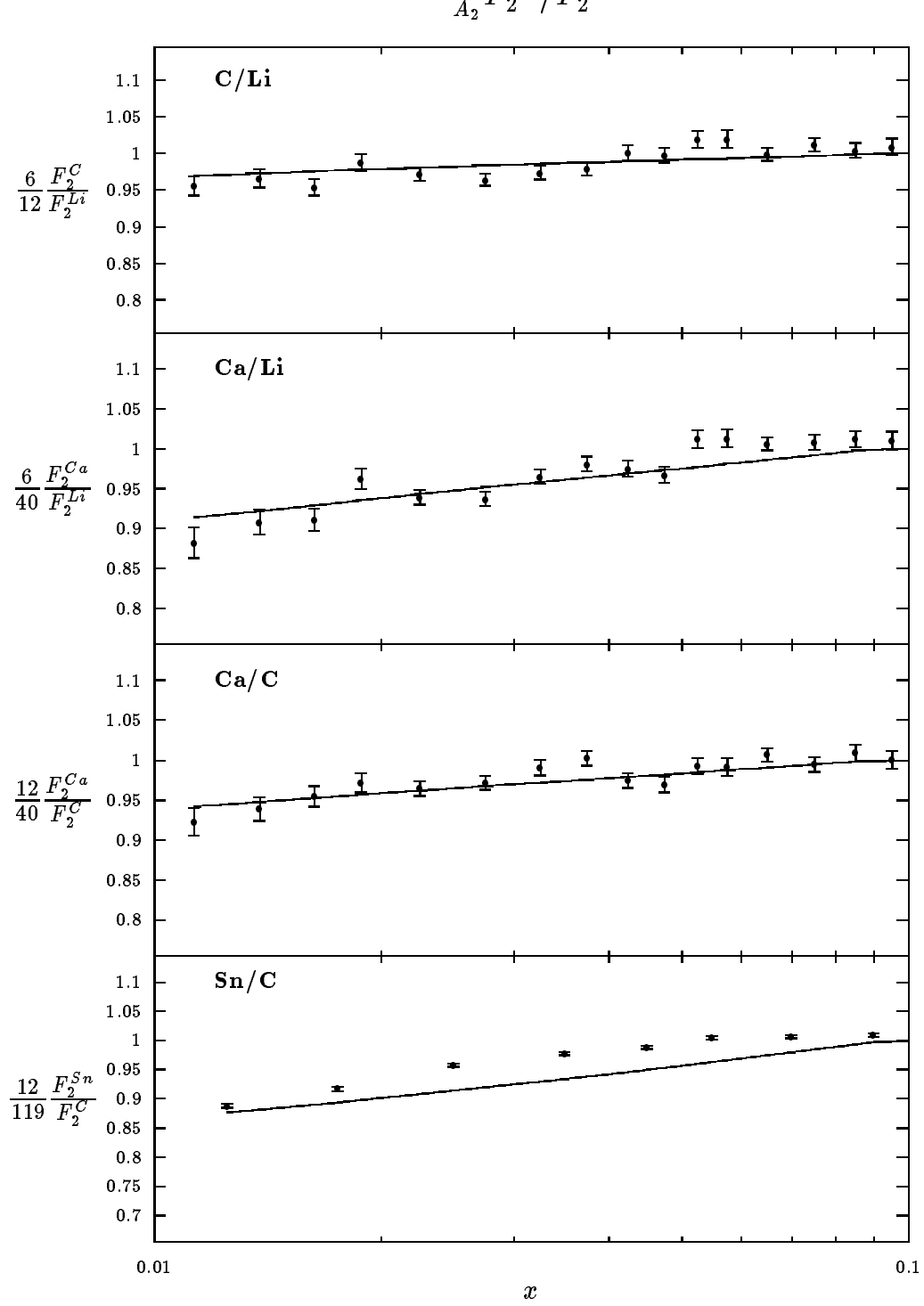


Fig. 4

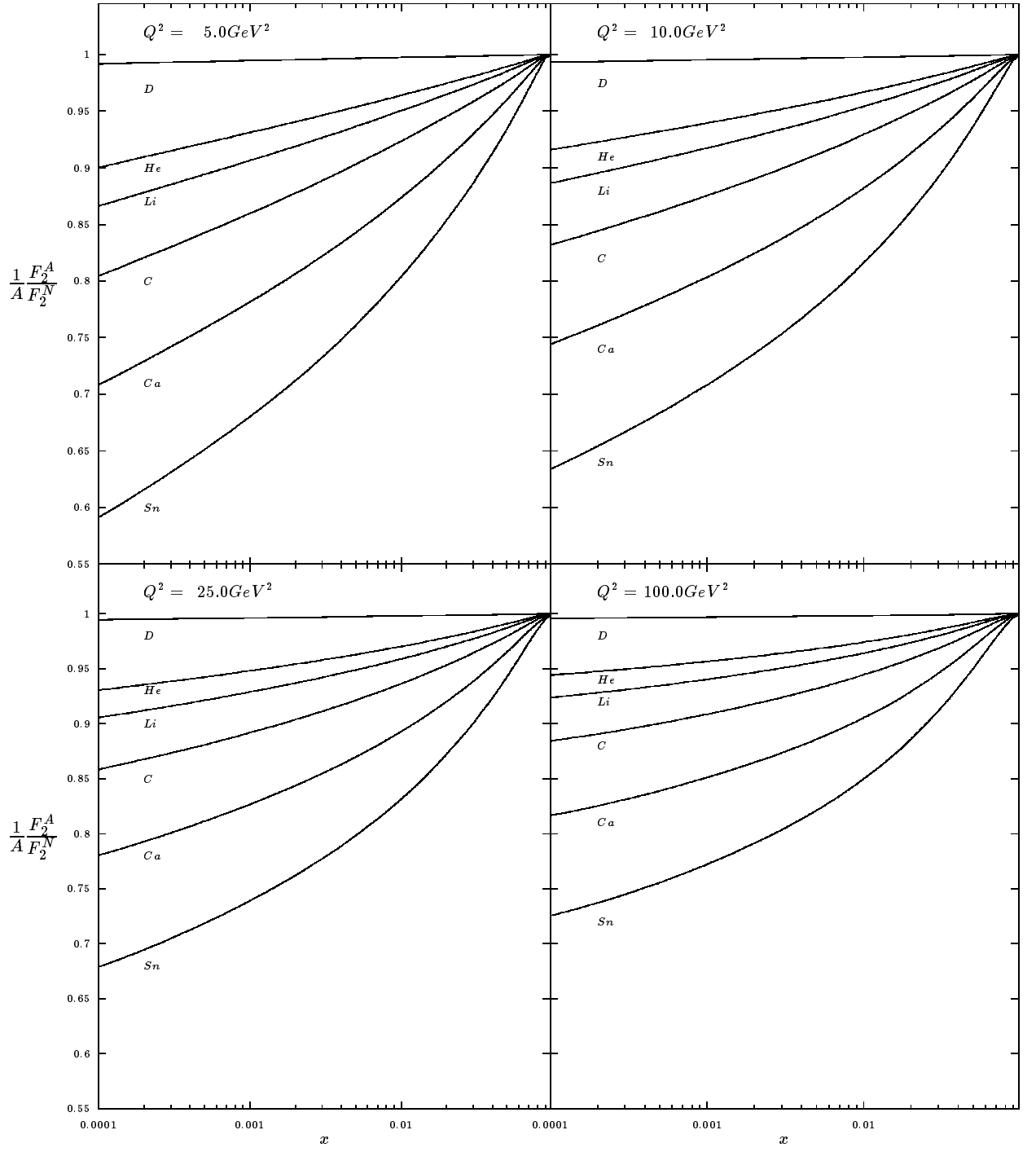


Fig. 5

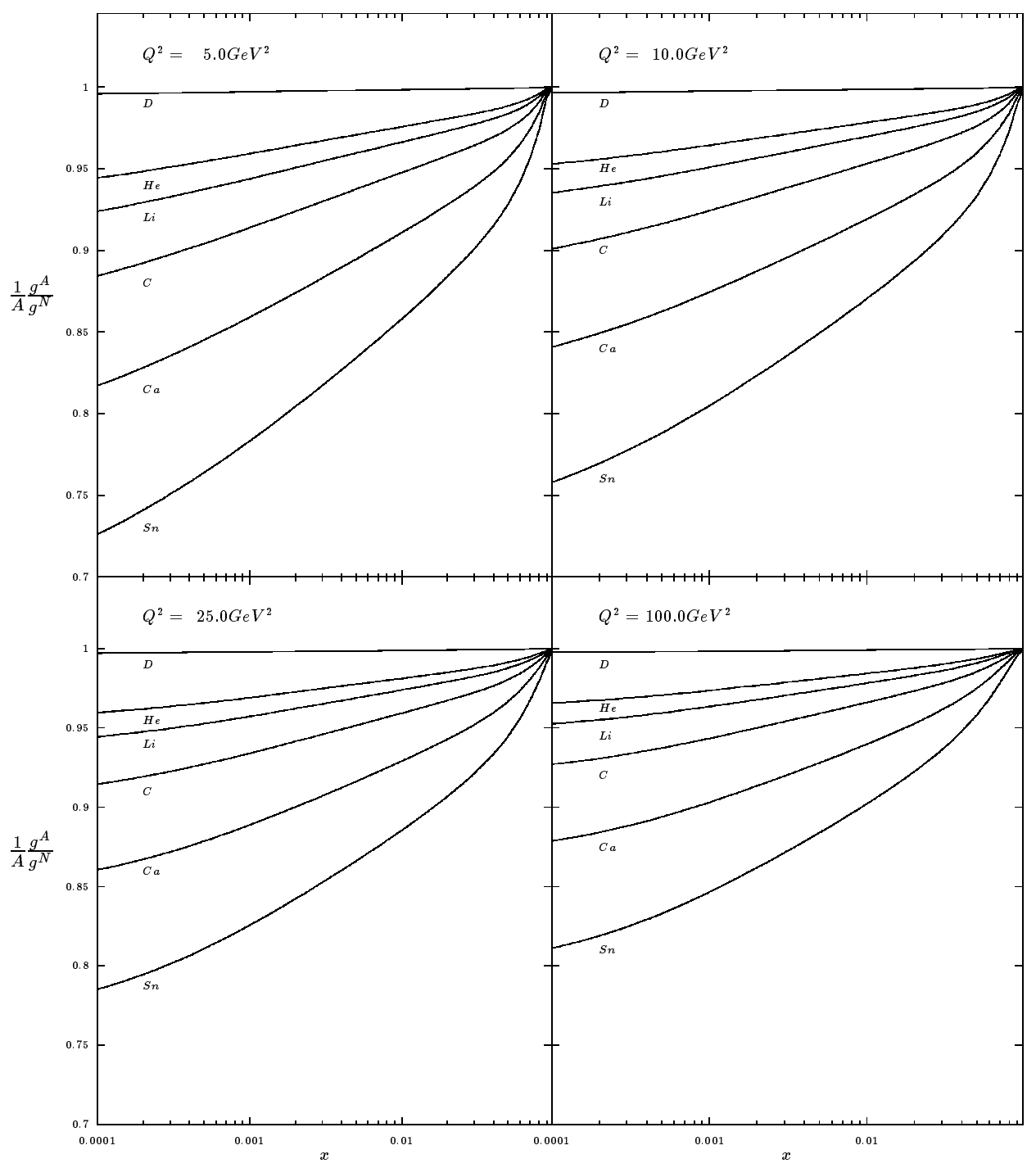


Fig. 6

$$\frac{12}{119} F_2^{Sn} / F_2^C$$

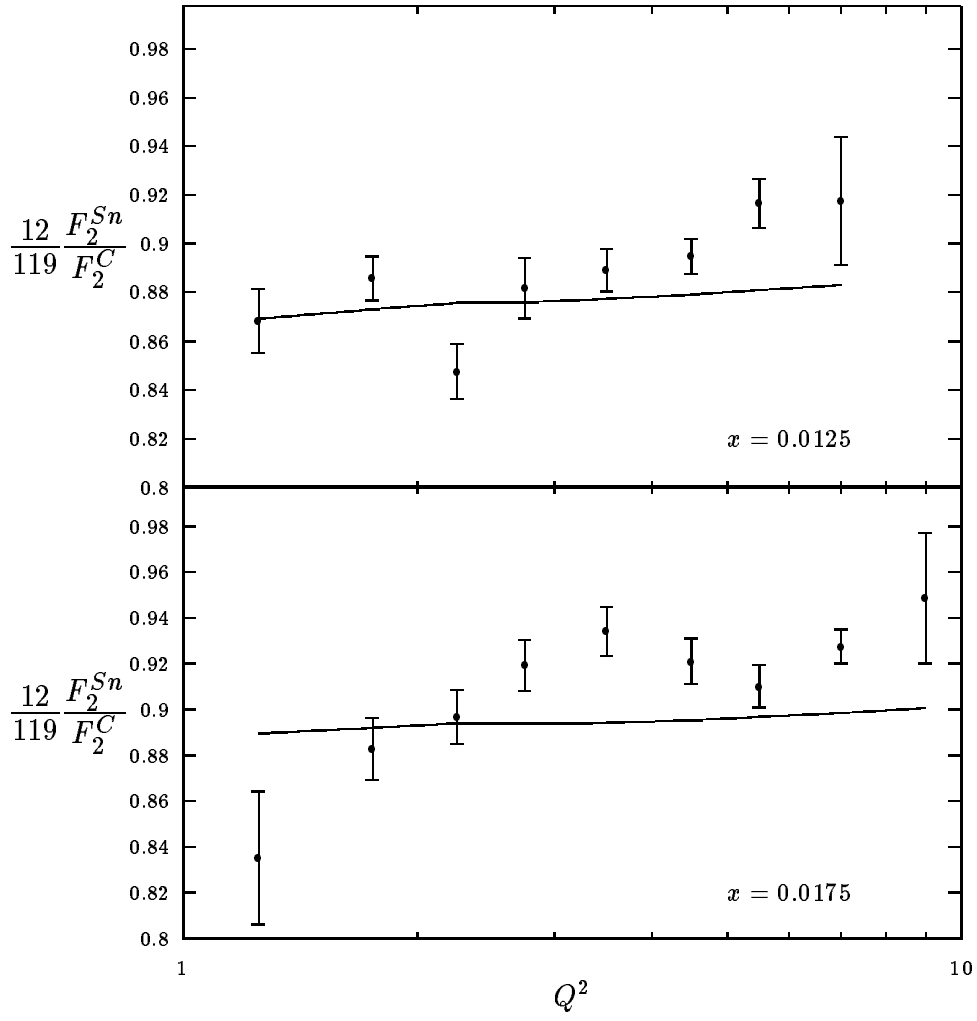


Fig. 7

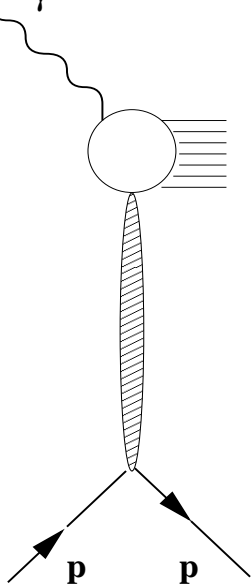


Fig. 1

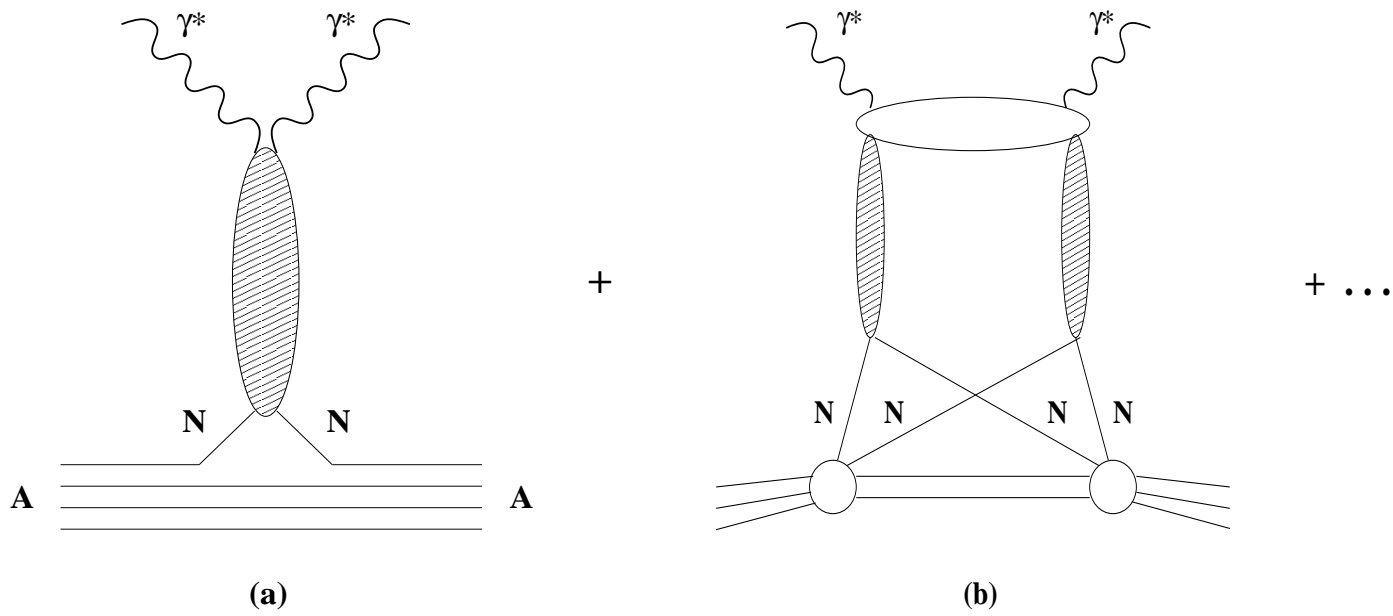


Fig. 2